IRAQI JOURNAL OF MATERIALS
Volume (5) Issue (2) April-June 2026, pp. 93-100
Published and Sponsored by American Quality for Scientific Publishing, Inc. (AQSP)

# Diffusion and Electrical Characteristics of Phosphorous-Doped Silicon Using Excimer Laser Pulses

**Hussein A. Jwad, Kadhem A. Abbas***

*Department of Physics, College of Science, Misan University, Misan Province, IRAQ*
** Corresponding author email: kadhim.aadim@yahoo.com*

**Abstract**
In this work, p-type silicon samples were doped with phosphorus using pulses of an ArF excimer laser. In order to separate the effects of the gas and the adsorbed layers on doping characteristics, experiments were performed using two different procedures; doping in $POCl_3$ ambient and doping using only adsorbed layers of $POCl_3$ on the sample surface. The lowest sheet resistance was obtained for samples doped in $POCl_3$ ambient. Activation energy for phosphorus evaporation from the silicon surface was determined. As well, electrical properties such as conductivity, carrier concentration and mobility were studied for the prepared samples at laser fluence of 2.5 $mJ/cm^2$. Results presented could be considered successfully to develop semiconductor-doping using ultraviolet-wavelength lasers.

***Keywords***: Laser-assisted diffusion, Silicon doping, Phosphorus dopants, Excimer laser
**Received:** November 2025; **Revised:** January 2026; **Accepted:** February 2026; **Published:** April 2026

## 1. Introduction

A potentially low cost doping alternative can be realized by using laser technology in combination with different doping sources such as gaseous, liquid or solid dopant materials [1-3]. Due to the laser radiation, the temperature locally increases, leading to an incorporation of the dopants by solid-state or liquid phase diffusion [6]. The type of laser used for the respective process varies with regard to wavelength and the pulse duration, ranging from the infrared (IR) to the ultraviolet (UV) and from below 100 fs pulses to continuous wave radiation, respectively [4-6]. The fundamental working principle is identical to most of the other known laser doping processes. The main difference lies in the application and structure of the doping precursor, which is performed prior to the process itself. The layers are always directly in touch with the silicon substrate, without any interlayers in between [7-9].

After the precursor deposition, the laser doping process itself starts. Based on the extensive research on laser melting and doping of semiconductors presented above, the laser doping process is hypothesized as follows. In the first stage, the laser irradiation heats up the precursor layer and the underlying silicon [10]. Either due to direct light absorption or, depending on the transparency of the precursor layer, due to heat transfer from the underlying silicon, the precursor evaporates and forms a dense vapor phase above the illuminated area. After then, the silicon surface melts and the melt front advances into the substrate. As soon as the silicon is molten, a liquid state diffusion process of dopant atoms starts. When the energy supply from the laser pulse ceases, the melt front reverses and the molten silicon recrystallizes epitaxially. As a consequence, a several 100 nm thick, doped area remains. The size of the doped area depends on the size of the laser focus on the substrate surface. In order to process larger areas, single laser spots are placed next to one another [11-13].

Laser melting of the silicon surface leads to an epitaxial regrowth of the silicon on the underlying substrate. The implanted impurity atoms are incorporated into substitutional lattice sites during the recrystallization with, their concentrations significantly exceeding the equilibrium solubility limit as well as, their segregation coefficients exceeding the equilibrium values. The concentration of implanted impurity atoms as well as the segregation coefficient depend on the recrystallization velocity, which is in the range of several meters per second [14-17].

At the same time to, or following the fundamental research, a number of authors reported results from "real" laser doping experiments, using different types of precursors and laser systems. There are some important results from these studies, there exists a threshold laser fluence for the onset of laser doping. This threshold coincides with the silicon melting threshold [18]. The depth of the laser-diffused layers increases linearly with the laser fluence [19]. Using a high number of repeated laser pulses leads

© All Rights Reserved 

to a rectangular doping profile, with the doping depth corresponding to the melting depth [20-23]. Infinite dopant sources can be realized using gaseous precursors [24], while deposited precursors mostly act as exhaustive sources, leading to a decrease of the maximum doping concentration upon multiple irradiation [22].

In spite of the vast scientific effort spent on characterizing the laser doping process at that time, and first solar cells that were produced [19], no real development of laser doping for photovoltaics was reported until the beginning the 21$^{st}$ century, when the solar industry commenced its incredible growth, and the search for cheaper solar cell production processes intensified [20].

As dimensions of very-large-scale-integrated (VLSI) devices continue to decrease, the main challenge in the area of junction formation involves decreasing the junction depth [25] while simultaneously decreasing the sheet resistance [26]. In order to meet these requirements, researchers have devised activation methods that can anneal the doped layer intensively for a short duration. Though rapid thermal annealing (RTA) [27] is effective in obtaining low resistivity, it also results in redistribution of highly diffusive dopants in silicon. Laser annealing has been developed as an alternative to RTA to repair the damage from ion implantation and to activate the dopants [28-31].

At the same time, silicon thin films, such as amorphous silicon or polycrystalline silicon on insulating substrates, silicon on insulator (SOI), or thin film transistor (TFT) on glass, have become attractive for flat panel displays and for system on panel (SOP) applications. In these applications, high-performance junction formation technique is required, as mentioned above. Therefore, the effect of laser activation on thin films of silicon such as single-crystal or polycrystalline silicon is of much interest [32-33].

The excimer laser assisted "*spin on*" doping technique uses a pulsed excimer laser to melt the silicon surface. The incorporation of dopant atoms into crystalline silicon and their electrical activation can be envisaged as follows. First, they are liberated from the coated solid thin film through thermal-assisted dissociation, where laser irradiation was used to heat the sample. Secondly, they undergo rapid diffusion at high temperature into the liquid phase silicon. Solid phase diffusion through the melt/solid interface is only possible for large pulse number. The molten layer regrows epitaxially, resulting in electrically active, damage-free layer [34-36].

During the ultrafast melt/regrowth process (<200 ns in duration) dopant incorporation is restricted to the liquid phase. This limits impurity profiles to the maximum melt depth, a parameter which can be controlled very accurately by adjusting the energy fluence of the laser on the sample. By using multiple pulses, dopant can be distributed evenly throughout the melted layer to form box-like profiles. These profiles, in conjunction with precise control of melt, enable exact vertical placement of the metallurgical junctions. The rapid thermal cycle, 1 billion times faster than a rapid thermal annealing (RTA), also allows emitter fabrication with no effect on the base-collector junction depth. The ability to place theses junction independently, in turn, allows simple fabrication of base regions less than 100 nm in width [37-40].

Reproducibility of the process is ensured by *in-situ* diagnostics which enable real-time prediction of the junction depth [41]. Masking is achieved using conventional lithography with an aluminum thin film to reflect the laser energy from regions where doping is not desired.

Among the n-type dopants of silicon, phosphorus has only been recently used in solid-source epitaxy growth systems [42]. Phosphorus doping is of interest for several reasons. The solid solubility of phosphorus in silicon is approximately 10 times higher than that of antimony in silicon, permitting the higher doping concentrations required in sub-micron devices and in tunneling devices. In addition, it has been suggested that in a silicon-based quantum computer, accurately positioned phosphorus donors would function as quantum bits (qubits) [43]. However, the high vapor pressure of phosphorus prevents its use as an elemental dopant in a molecular beam epitaxy (MBE) growth system. There have been previous investigations of coevaporation of highly phosphorus-doped silicon, [33] and reports of the use of GaP in a Knudsen cell [44]. However, a comprehensive study of phosphorus doping of silicon using GaP is lacking.

Impurity doping to silicon by decomposing $BCl_3$, $PCl_3$, $B(CH_3)_3$ and $Al(CH_3)_3$ using excimer lasers has been described [45,46]. Also, it had been shown from experiments using excimer lasers that both photochemical decomposition of the doping gas and thermal decomposition of adsorbed layers contribute to the formation of dopant atoms [47]. However, the absorption properties of the adsorbed layers may be different for different laser wavelengths. In other words, the adsorbed layers are decomposed, as well as the doping gas, photochemically or thermally by excimer laser irradiation. Then, if two different laser wavelengths are used, the effect that photochemical decomposition has on doping cannot be separated from the doping using the adsorbed layers. It is important to perform the excimer

© All Rights Reserved

laser doping using same wavelength in order to investigate the effect of photochemical decomposition [48-52].

In this work, we perform impurity doping using ArF excimer laser with a doping gas that is adsorbed at the wavelength of laser (193nm), and investigate the influence of photochemical decomposition on doping characteristics. Since we compare doping in gas ambient with that using only the adsorbed layers at the same laser wavelength, we are able to separate the effect that photochemical decomposition of a doping has on dopant incorporation. As well, the activation energy, electrical conductivity, carrier concentration and mobility for some of the prepared sampled were determined at the highest value of laser fluence.

**2. Experimental Part**

Phosphoryl chloride ($POCl_3$, commonly called phosphorus oxychloride) was used as a doping gas. It is a colorless liquid with freezing point of 1 °C and boiling point 106 °C, so the liquid range is very similar to water. It hydrolyses in moist air releasing "phosphoric acid" and choking fumes of hydrogen chloride. In the semiconductor industry, $POCl_3$ is used as a safe liquid phosphorus source in diffusion processes. The phosphorus acts as a dopant used to create n-type layers on a silicon wafer. It is typical as the liquid diffusion source of phosphorus and it is easy to use. $POCl_3$ was loaded into a doping chamber through a reservoir by using nitrogen gas as the carrier. The reservoir was kept at 298 K and $POCl_3$ vapor pressure was estimated to be about 40 torr [53,54]. Flow rate of nitrogen gas was 0.1 liters/min.

The absorption characteristic of $POCl_3$ gas was estimated by comparing the intensity of ultraviolet light through the sample gas and through a nitrogen gas which is a reference gas. These gases were enclosed in 1cm-length cell with quartz windows. We have used a scanning monochromator with a heavy hydrogen lamp as a light source, and the transmission intensity of the light through the gas was measured by a photomultiplier. The absorption characteristic of $POCl_3$ adsorbed layers on quartz windows of the cell was also measured.

The absorption characteristic through the cell filled with $POCl_3$ gas includes both absorptions of the gas and the adsorbed layers on the windows. Then, the absorption characteristic of only the gas was evaluated by comparing the above characteristic with that of only the adsorbed layers. An ArF excimer laser with pulse duration of 17 ns at 193 nm was operated at 2 Hz. The focused laser beam was directed onto sample with a beam size of about 14mm$^2$. Samples used were p-type (100) single crystal silicon with a resistivity of 3-5 Ω.cm. The sample surface was chemically cleaned using basic peroxide ($NH_4OH:H_2O_2:H_2O$ = 1:1:5) and acid peroxide ($HCl:H_2O_2:H_2O$ = 1:1:5) process with an HF dip and a deionized $H_2O$ rinse.

In order to separate the effects of the gas and the adsorbed layers on doping characteristics, experiments were performed by two different procedures; (i) doping in $POCl_3$ ambient, and (ii) doping using only adsorbed layers of $POCl_3$ on the sample surface. In the first one, $POCl_3$ gas flowed during the irradiation of ArF excimer laser, while in the latter, $POCl_3$ gas was purged from a doping chamber using nitrogen after loading the gas. By this procedure, dopant atoms are supplied from only the adsorbed layers during the excimer laser doping.

Sheet resistance of the doped area was measured by the four-point probe method. Carrier concentration profiles were determined by the differential resistivity measurement using the four-point probe method with an anodic oxidation, which was carried out in phosphoric acid ($H_3PO_4$) solution. For the sheet resistance characterization, polished p-type CZ and FZ samples are used. The samples undergo the coating step on a laboratory spin-coater followed by a bakeout step on a hotplate at a temperature 300 °C for 12 minutes. After the bakeout, the layer thickness for the two groups of prepared samples amounts to about 100 nm and 400 nm due to the difference in viscosity. Following the bakeout the samples are ready for laser irradiation. The range of the laser pulse energy densities extends from 0.1 to 2.5 J/cm$^2$. In order to avoid sample to sample fluctuation, every sample carries multiple areas irradiated with the varying laser parameters. After the laser process, a cleaning step in diluted Hydrofluoric Acid (5% HF) removes the residues of the precursors and cleans the samples.

The sputtered phosphorous layers are prepared with the traditional indentation toughness (TIT) method. By changing the deposition time, the thickness of the phosphorous layers is adjusted within 2-30 nm. After coating, the samples directly receive the laser irradiation with 0.8-2.5 J/cm$^2$, without any necessary annealing step. After cleaning, the sheet resistance data for both precursor types is measured with a four point probe (FPP) setup. For every laser parameter five individual measurements are averaged across the irradiated area.

© All Rights Reserved

### 3. Results and Discussion

Both absorption characteristics of $POCl_3$ gas and the adsorbed layers in the ultraviolet region are shown in Fig. (1). $POCl_3$ gas had a large absorption at about 193nm, and the absorption coefficient is estimated to be 0.29 $cm^{-1}$ ($POCl_3$ 40 torr) at 193nm. Then, $POCl_3$ gas can be decomposed by ArF excimer laser irradiation despite that this absorption causes the decrease of the incident laser energy density at the surface of sample in $POCl_3$ ambient. The adsorbed layers have absorption at about 200 nm. Then, the adsorbed layers can be also decomposed photochemically by the irradiation of ArF excimer laser.

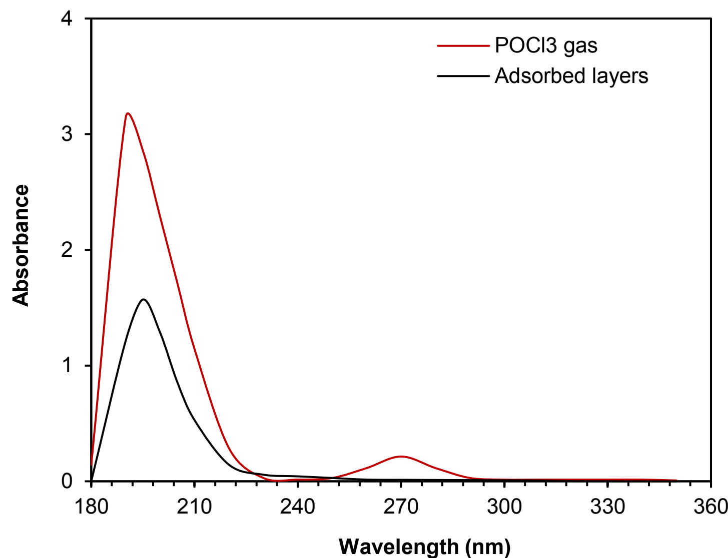


**Fig. (1) UV absorption spectra of $POCl_3$ gas and the adsorbed layers at room temperature**

Figure (2) shows the dependence of sheet resistance on the number of pulses. Curve (a) shows the doping in $POCl_3$ ambient at 1.2 J/cm$^2$, and curves (b) and (c) show the doping using the adsorbed layers at 0.8 and 1.2J/cm$^2$, respectively. The lowest sheet resistance was obtained for samples doped in $POCl_3$ ambient. Because of the decrease of laser intensity in $POCl_3$ gas, incident laser energy density of 1.2J/cm$^2$ is estimated to be 0.9 J/cm$^2$ on the surface of sample in $POCl_3$ ambient. Hence, the beam energy density on the surface of sample is almost same between doping in $POCl_3$ ambient at 1.2 J/cm$^2$ and that using the adsorbed layers at 0.8 J/cm$^2$. Therefore, the difference in sheet resistance between both cases is caused by the incorporation of dopant atoms produced by photochemical decomposition of $POCl_3$ gas into silicon. As for the doping using the adsorbed layers (curves of b and c), sheet resistance of samples doped at 1.2 J/cm$^2$ is lower than that doped at 0.8 J/cm$^2$. Because melting time becomes longer as beam energy density increases [55], more incorporations of dopant atoms from the adsorbed layers into silicon cause the low sheet resistance. Meanwhile, the sheet resistance decreases with increasing the number of pulses at both beam energies. It indicates that there are the adsorbed layers on the silicon surface after laser irradiation.

Carrier concentration profiles for samples doped at 1.2J/cm$^2$ in $POCl_3$ ambient are shown in Fig. (3). Compared with the doping using the adsorbed layers, the surface concentrations are nearly constant until 150 pulses. Because more dopant atoms are supplied by photochemical decomposition of $POCl_3$ gas in addition to the adsorbed layers, the surface concentration saturates earlier than the case of doping using only the adsorbed layers. The total quantities of impurity as a function of the number of pulses are shown in Fig. (4). The total quantity for doping in $POCl_3$ ambient (green line) is much larger than that of doping using the adsorbed layers (red line). It is clear that the difference is caused by dopant atoms supplied from only the gas phase, which is subtracted from the quantity of doping using the adsorbed layers from that of doping in $POCl_3$ ambient. The result is nearly comparable to the green line obtained from the doping in the gas ambient. It is found that dopant atoms produced by photochemical decomposition in the gas phase are the dominant source of supply into silicon.

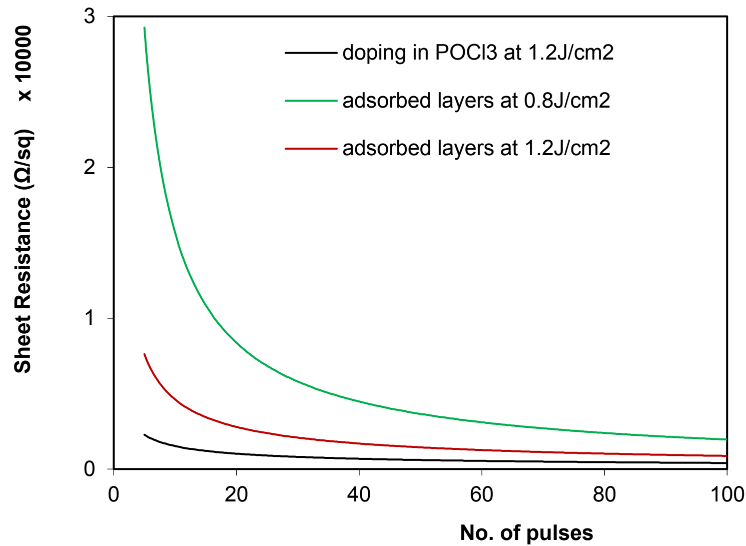


**Fig. (2) Sheet resistance vs. the number of pulses for doping in $POCl_3$ ambient at 1.2J/cm$^2$, using the adsorbed layers at 0.8J/cm$^2$, and using the adsorbed layers at 1.2J/cm$^2$**

The activation energy for the phosphorus evaporation can be determined by plotting the logarithm of remaining phosphorus atoms ($P_{rem}$) versus reciprocal temperature (1/T) [56], as shown in Fig. (5). This plot is only valid since the time at temperature for each sample is the same. The activation energy for phosphorus evaporation has been determined to be 2.07±0.23 eV or 199±22 kJ/mol. This corresponds very well to prior determinations. Figure (6) shows the electrical conductivity of poly-silicon films with respect to the number of laser shots. The step-up irradiation was applied to the laser energy density of 2.5 mJ/cm$^2$ and the number of shots at each step was varied from one to 10. The electrical conductivity increases with increasing laser energy density, except for a drop at five shots.

The prepared samples were also examined by the Hall effect measurement, and the result is shown in Figs. (7) and (8). The carrier concentration increases from $7.4 \times 10^{13}$ to $3.3 \times 10^{14}$ cm$^{-3}$ as the number of laser shots is increased. The carrier mobility decreases as the number of laser shots is increased from one to five, shows a minimum value at five shots, then increases with increasing number of laser shots. The number of laser shots is also important in the electrical characteristics of the polycrystalline silicon films [57].

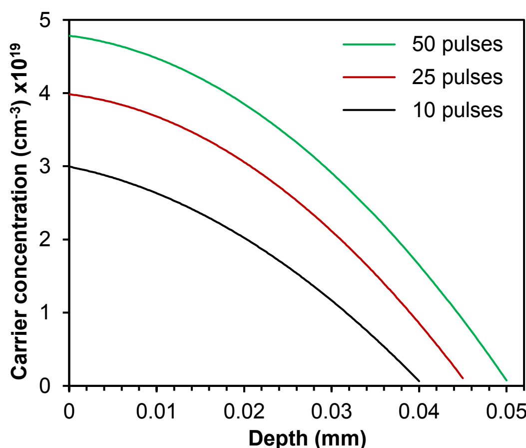


**Fig. (3) Carrier concentration profiles for samples doped at 1.2J/cm$^2$ in $POCl_3$ ambient**

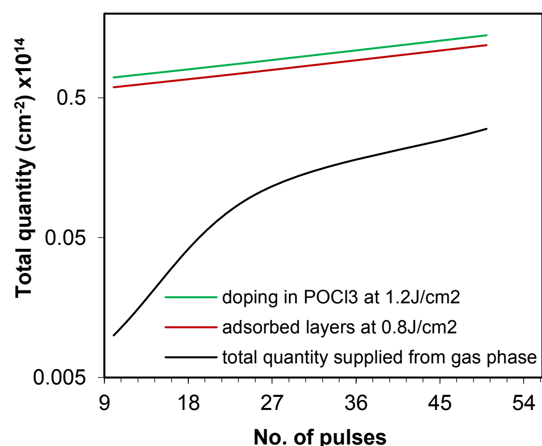


**Fig. (4) Total quantity vs. the number of pulses (green line) doping in $POCl_3$ ambient at 1.2J/cm$^2$, (red line) using adsorbed layers at 0.8J/cm$^2$, and (black line) the total quantity supplied from only the gas phase**

© All Rights Reserved

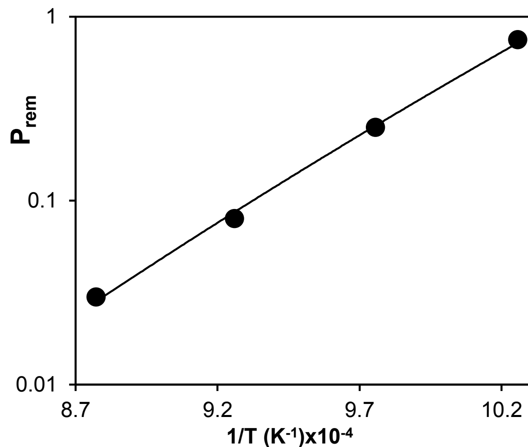


Fig. (5) Variation of the remaining phosphorus atoms ($P_{rem}$) with reciprocal temperature (1/T) to determine of the activation energy for phosphorus evaporation from the silicon surface

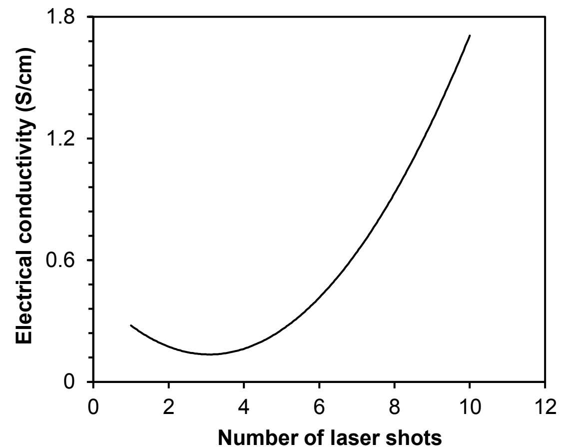


Fig. (6) Variation of electrical conductivity with the number of laser shots at laser fluence of 2.5 mJ/cm$^2$

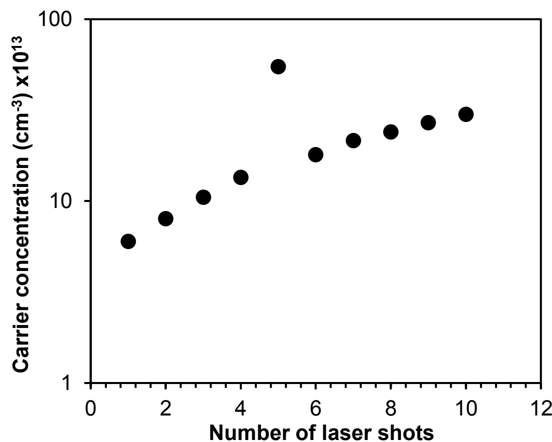


Fig. (7) Variation of carrier concentration with the number of laser shots at laser fluence 2.5mJ/cm$^2$

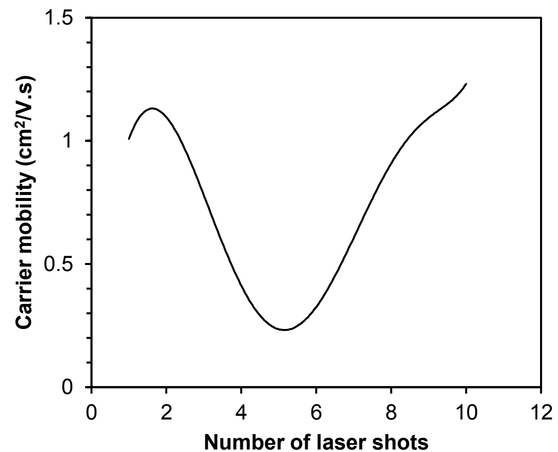


Fig. (8) Variation of carrier mobility with the number of laser shots at laser fluence 2.5mJ/cm$^2$

## 4. Conclusion

From the experiments of doping in $POCl_3$ ambient and that using the adsorbed layers formed on the silicon surface, it could be concluded that dopant atoms produced by photochemical decomposition of $POCl_3$ influence the doping characteristics. In the case of doping in $POCl_3$ ambient, the surface concentration is nearly constant. It is due to a large quantity of dopant atoms supplied from the gas ambient.

## References

[1] F. Han et al., "Achieving ultrahigh aluminum melt corrosion resistance via laser-induced nanoeutectic architectures in WMoTaNb high-entropy alloy coatings", Mater. Design, 261 (2026) 115325.
[2] T. Hu et al., "Effects of oxygen-fuel velocity ratio on soot formation and flame structure in $CH_4$-$CO_2$-$O_2$ inverse diffusion flames", Fuel, 412 (2026) 138172.
[3] J. Guo et al., "Stability and NO formation of ammonia/methane non-premixed flames under $O_2/CO_2$ environments", Combus. Flame, 283 (2026) 114621.
[4] M.N. Müller et al., "Influence of volumetric multi-kHz laser irradiation on soot particle measurements in laminar diffusion flames", Appl. Phys. B: Lasers Opt., 131(11) (2025) 215.
[5] M. Soleimani et al., "Ultra-low-temperature sintering of $TiO_2$ via grain boundary diffusion enabled by nanosecond laser irradiation", Mater. Today Nano, 33 (2026) 100732.
[6] Z. An et al., "Flame/droplet interaction and combustion mode in a liquid ammonia jet flame", Combus. Flame, 283 (2026) 114603.
[7] O.A. Hamadi, "Profiling of Antimony Diffusivity in Silicon Substrates using Laser-Induced Diffusion Technique", *Iraqi J. Appl. Phys. Lett.,* 3(1) (2010) 23-26.
[8] L. Qi et al., "The Accelerated Topological Laser Induced by Non-Hermitian Topological Flat Band in The Dimerized Lattice", Adv. Quantum Technol., 8(11) (2025) e00354.

© All Rights Reserved

[9] G.D. Tsibidis, “Influence of inter-pulse delay and geometric constraints on damage and optical characteristics in thin metal targets irradiated by double ultrashort laser pulses”, Appl. Surf. Sci., 732 (2026) 166516.
[10] A. Mehrvarz et al., “Mechanistic insights into laser-structured NMC811 cathodes for fast-charging lithium-ion batteries”, J. Energy Stor., 143 (2026) 119747.
[11] A.A.K. Hadi, O.A. Hamadi and R.A. Markub, “Heat-annealed enhanced-diffusion of silver in gallium arsenide”, *Mustansiriya Univ. J. Edu.*, 3(1) (2001) 35-44.
[12] X. Yang et al., “Effect and mechanisms of ethanol addition on soot formation in high-pressure n-heptane laminar diffusion flames”, *Fuel*, 418 (2026) 138660.
[13] C. Ji et al., “Mechanisms of femtosecond laser plasmonic micro-welding between sapphire and rough SiC ceramics with natural stacking using ultrafast optical imaging”, *J. Manufact. Process.*, 156 (2025) 219-236.
[14] G. Debnath and B. Vasu, “FEM simulation of dual-phase irradiance for laser-induced hyperthermia in skin tumors: A multi-site GNP injection approach”, *Int. Commun. Heat Mass Transfer*, 172 (2026) 110507.
[15] C.-C. Chiang and P.N. Immanuel, “P–N Nanoporous Silicon Fabrication Using Photoelectrochemical Etching and Ultrasonic Vibration and Liquid-Phase Bonding for Optoelectronic Applications”, Micromachines, 17(1) (2026) 73.
[16] O.A. Hammadi, “Finite-Element Analysis of Laser-Induced Diffusion of Metallic Dopants in Silicon for Microelectronics Applications”, *Procedia Mater. Sci.*, 15 (2021) 101200.
[17] P. Chu et al., “One-point calibration of underwater double-pulse laser-induced breakdown spectroscopy”, *Spectrochimica Acta B: Atom. Spectro.*, 237 (2026) 107455.
[18] S. Rathi et al., “CTx001 for Geographic Atrophy: A Gene Therapy Expressing Soluble, Truncated Complement Receptor 1 (Mini-CR1)”, *Ophthalmol. Sci.*, 6(1) (2026) 100980.
[19] H. An, J. Wang and Z. Xu, “Controllable Material Removal via Diffusion-Assisted Etching at the Atomic Scale”, *Nanomanufact. Metrol.*, 8(1) (2025) 26.
[20] W. Zhao et al., “Laser-induced gas-assisted debonding in advanced packaging applications”, *Opt. Laser Technol.*, 199 (2026) 114956.
[21] J. Panda et al., “Defect-engineered activated bimetallic MOFs on laser-induced graphene for enhanced $NO_2$ sensing”, *J. Environ. Chem. Eng.*, 14(1) (2026) 120484.
[22] J.-Z. Qin et al., “In-situ monitoring of liquid-liquid reaction kinetics by planar laser-induced fluorescence (PLIF) technique”, *Colloids Surf. A: Physicochem. Eng. Aspects*, 726 (2025) 138145.
[23] V. Esposito et al., “Soot and nanoparticle formation in ethylene counterflow diffusion flames: effects of nitrogen dilution and strain rate”, *Combus. Flame*, 284 (2026) 114631.
[24] Y. Zhou et al., “Nanosecond UV laser-induced subsurface damage mechanism and mechanical responses for cemented tungsten carbide”, *Int. J. Refract. Metals Hard Mater.*, 133 (2025) 107334.
[25] O.A. Taqatqa et al., “Laser-textured polymer-metal bonding: A combined experimental and computational approach to enhanced mechanical bond strength”, *Compos. Struct.*, 381 (2026) 120038.
[26] C. Zhou et al., “Laser-Induced High-Density Bi–F–C Sites to Unleash Potent $Li^+$ Adsorption for Stable Lithium Anodes”, *Adv. Mater.*, 38(11) (2026) e17701.
[27] W. Mo et al., “Flame Structure and Flame–Flow Interaction in a Centrally Staged Burner Featuring a Diffusion Pilot”, *Aerospace*, 12(11) (2025) 1019.
[28] Y. Xu et al., “Study on PAH and soot formation in 2,5-dimethylfuran counterflow diffusion flames with ammonia addition”, *Fuel*, 406 (2026) 137193.
[29] F. Huang et al., “Femtosecond laser induced electronic plasma ultrafast dynamics and material damage in 6H-SiC”, *Opt. Commun.*, 598 (2026) 132618.
[30] K. Minami et al., “Generation of high-aspect-ratio 3C-SiC nanowires and evaluation of their potential as battery materials”, *Mater. Design*, 259 (2025) 114872.
[31] N. Nedyalkov et al., “Laser-induced gold and silver nanoparticle implantation in glass for fabrication of plasmonic structures with multiple use”, *Opt. Laser Technol.*, 191 (2025) 113361.
[32] S. Mittelmann et al., “Femtosecond Laser-Induced Ablation – Quadrupole Mass Spectrometry (fs-LIA-QMS) experiment for the detection of trapped hydrogen isotopes and helium in nuclear fusion relevant materials”, *Spectrochimica Acta B: Atom. Spectro.*, 233 (2025) 107283.
[33] H. Gao et al., “N, B, and S heteroatom-doped laser-induced porous PES-derived graphene for high-performance supercapacitors”, *New J. Chem.*, 50(10) (2026) 4533-4542.
[34] O.A. Hamadi et al., “Characteristics of Cr diffusion in p-type silicon”, *Eng. Technol. J.*, 21(2) (2002) 55-59.
[35] H.G, Ryu et al., “Comparative Morphometric and Histometric Evaluation of Power-Dependent Tissue Ablation Using Fractional Carbon Dioxide Laser”, *Clinic. Cosmetic Investig. Dermatol.*, 18 (2025) 1901-1907.
[36] R. Zhang et al., “Study of near-infrared semiconductor laser irradiation of biological skin tissues for non-lethal laser thermal dispersion”, *Opt. Laser Technol.*, 190 (2025) 113189.
[37] A. Suea-Ngam et al., “Functionalized laser-induced graphene enabled ultrasensitive electroimmunoassay for rapid hepatitis B virus detection”, *Bioelectrochem.*, 169 (2026) 109179.
[38] J. Cai et al., “Tuning laser-induced optical breakdown and cavitation through the ionic environment in aqueous media”, *Phys. Fluids*, 37(12) (2025) 123353.
[39] K. Li et al., “Mechanisms of femtosecond laser-induced selective hierarchical biomimetic texturing on the wettability and adhesive performance of CFRP surfaces”, *Compos. B: Eng.*, 313 (2026) 113401.
[40] S. Zhao et al., “Groundwater and ferromanganese oxide-coated calcareous concretion release excess radon to the southwestern Yellow Sea”, *Estuarine Coast. Shelf Sci.*, 329 (2026) 109664.
[41] O.A. Hamadi et al., “Ohmic characteristics of Ni/Si contact produced by laser-induced diffusion technique”, *Almustansiriya J. Sci.,* 12(6) (2001) 475-483.
[42] L. Du et al., “Laser-induced pitch-derived carbon with highly conductive graphite domains for high-performance lithium/potassium storage”, *Carbon*, 250 (2026) 121303.
[43] H. Xu et al., “In-situ laser diagnostics of turbulent premixed $H_2$/air flame structure and stability based on OH-PLIF and spontaneous Raman spectroscopy”, *Int. J. Hydro. Energy*, 198 (2026) 152723.

© All Rights Reserved

[44] C.D. Carter et al., “$CH_3$ photo-fragmentation laser-induced fluorescence for turbulent flame diagnosis”, *Combus. Flame*, 282 (2025) 114529.
[45] Y. Tao et al., “Effect of different Ti doping modes on diamond/Cu–Sn composites forming via laser powder bed melting”, *Int. J. Refract. Metals Hard Mater.*, 133 (2025) 107385.
[46] Z. Mingliang et al., “AI-driven entropy optimization in bio-convective third-grade nanofluid flow with electroosmotic effects”, *Int. Commun. Heat Mass Transfer*, 172 (2026) 110204.
[47] G. Long et al., “Fabrication of hedgehog-like micro/nanostructure arrays with anti-reflection on copper surface by femtosecond laser and thermal oxidation”, *J. Alloys Compd.*, 1054 (2026) 186275.
[48] J.T. Solomon, R. Lockyer and N. Hackworth, “Flow dynamics of a 15kHz supersonic coaxial injector: insights from PLIF and PIV measurements”, *Aeronaut. J.*, 129(1341) (2025) 3165-3183.
[49] W. Xu et al., “The effect of evaporation on laser-induced wetting and spreading behaviors of Mg alloy on Cu-coated steel substrates”, *Opt. Laser Technol.*, 195 (2026) 114559.
[50] H. Du et al., “Investigation of ammonia addition on soot radiation effects in n-heptane laminar diffusion flames at elevated pressure”, *Fuel*, 405 (2026) 136643.
[51] W. Wei et al., “Spatiotemporal dynamics of $TC_4$ titanium alloy surface plasma induced by femtosecond laser”, *Opt. Laser Technol.*, 196 (2026) 114722.
[52] C. Ma et al., “Controlled interfacial debonding based on laser induced deformation-impact coupling effect for advanced packaging”, *Appl. Surf. Sci.*, 721 (2026) 165350.
[53] H. Zhang et al., “Effect of laser processing severity on the strength and durability of 5052 aluminum alloy bonded joints”, *Opt. Laser Technol.*, 196 (2026) 114725.
[54] P. Chen et al., “Laser-stepwise-induced graphene with reduced sheet resistance enables electromagnetic shielding manipulation”, *Nano Res.*, 18(11) (2025) 94908018.
[55] P. Florian et al., “Fabrication, s-SNOM Characterization and in vitro Testing of Laser-Induced Periodic Surface Structures for Dental Abutment Applications”, *IEEE Photon. J.*, 18(2) (2026) 3700113.
[56] S. Utadiya et al., “Photothermal digital holography for imaging and characterization of multilayered structures”, *Opt. Exp.*, 33(25) (2025) 53028-53045.
[57] X. Zhao et al., “Collinear Pulse Train PLD: Fabrication of High-Refractive-Index-Difference $TiO_2$/ZnO Multilayers with Multifunctional Applications”, *Appl. Sci. (Switzerland)*, 16(3) (2026) 1354.

© All Rights Reserved ISSN (print) 2958-8960 (online) 3006-6042 